Measurement of key resonances for the ^{24}Al$(p,\gamma)^{25}$Si reaction rate using in-beam γ-ray spectroscopy

B. Longfellow,[1,2] A. Gade,[1,2,3] B. A. Brown,[1,2] W. A. Richter,[4,5] D. Bazin,[1] P. C. Bender,[1,*] M. Bowry,[1,†] B. Elman,[1,2] E. Lunderberg,[1,2] D. Weisshaar,[1] and S. J. Williams[1,‡]

[1]*National Superconducting Cyclotron Laboratory, Michigan State University, East Lansing, Michigan 48824, USA*
[2]*Department of Physics and Astronomy, Michigan State University, East Lansing, Michigan 48824, USA*
[3]*The JINA Center for the Evolution of the Elements, Michigan State University, East Lansing, Michigan 48824, USA*
[4]*iThemba LABS, P.O. Box 722, Somerset West 7129, South Africa*
[5]*Department of Physics, University of Stellenbosch, Matieland 7602, South Africa*

(Received 10 January 2018; revised manuscript received 4 March 2018; published 4 May 2018)

Energy levels and branching ratios for the *rp*-process nucleus ^{25}Si were determined from the reactions ^{9}Be(^{26}Si,^{25}Si)X and ^{9}Be(^{25}Al,^{25}Si)X using in-beam γ-ray spectroscopy with both high-efficiency and high-resolution detector arrays. Proton-unbound states at 3695(14) and 3802(11) keV were identified and assigned tentative spins and parities based on comparison to theory and the mirror nucleus. The ^{24}Al$(p,\gamma)^{25}$Si reaction rate was calculated using the experimental states and states from charge-dependent USDA and USDB shell-model calculations with downward shifts of the $1s_{1/2}$ proton orbital to account for the observed Thomas-Ehrman shift, leading to a factor of 10–100 increase in rate for the temperature region of 0.22 GK as compared to a previous calculation. These shifts may be applicable to neighboring nuclei, impacting the proton capture rates in this region of the chart.

DOI: 10.1103/PhysRevC.97.054307

I. INTRODUCTION

The structure of neutron-deficient nuclei plays a crucial role in nucleosynthesis during explosive stellar hydrogen burning through the *rp* process, which consists of sequences of rapid proton captures and β decays [1]. Near the proton drip line, the Q values of (p,γ) reactions are low and the reaction rates are dominated by single resonances and direct capture contributions. For many nuclei on the *rp*-process path, due to the lack of data, estimates of the proton-capture rates have been based on input from theory and mirror nuclei [2–4] or, for nuclei with $T_z = -1$, the isobaric mass multiplet equation together with data on nuclei with $T_z = 0,1$ [5–7].

At the beginning of the *rp* process, there is breakout from the hot CNO cycle into the Ne-Na region. The flow out of the Ne-Na cycle proceeds via chains involving the reaction ^{24}Al$(p,\gamma)^{25}$Si [2,8]. Not much is known about excited states in ^{25}Si, in particular those relevant to the reaction rate calculation just above the proton separation energy of $S_p = 3414(10)$ keV [9]. ^{25}Si has been studied by Benenson *et al.* using the ^{28}Si(^{3}He,^{6}He)^{25}Si reaction, which populated one state in the relevant energy range at 3820(20) keV with unmeasured spin and parity [10]. Consequently, calculations of the ^{24}Al$(p,\gamma)^{25}$Si reaction rate such as those by Herndl *et al.* have relied on the energies and spin-parity assignments of analog states in ^{25}Na [3]. Varying this reaction rate up and down by factors of 100 was found to affect the nucleosynthesis of ^{28,29,30}Si, ^{33,34}S, and ^{36}Ar by up to 40% [11]. The abundance ratios of ^{29,30}Si to ^{28}Si are important for presolar grain identification [12]. In a 1995 conference proceeding, the preliminary observation of a resonance in ^{25}Si at 3.7 MeV dominating the reaction rate of ^{24}Al$(p,\gamma)^{25}$Si in the temperature range up to 10^9 K was presented [13,14]. See Ref. [8] for a more recent sensitivity study of the breakout reactions from the hot CNO cycle discussed in Ref. [14].

In the present paper, excited states in ^{25}Si are populated and identified using in-beam γ-ray spectroscopy with both high-efficiency and high-resolution detector arrays following the reactions ^{9}Be(^{26}Si,^{25}Si)X and ^{9}Be(^{25}Al,^{25}Si)X. Two resonances above the proton separation energy were observed from their γ-ray decays. Our ^{25}Si level scheme is compared to shell-model calculations and the mirror nucleus [15,16] and an updated ^{24}Al$(p,\gamma)^{25}$Si reaction rate calculation is presented.

II. EXPERIMENT

The data sets presented in this paper originate from three different experiments performed at the National Superconducting Cyclotron Laboratory [17]. For the most recent measurement, a 150 MeV/u primary beam of ^{36}Ar was used to produce a secondary beam cocktail including ^{26}Si (14%) and ^{25}Al (30%) by projectile fragmentation on a 550 mg/cm^2 ^{9}Be target which

*Present address: Department of Physics, University of Massachusetts Lowell, Lowell, Massachusetts 01854, USA.
†Present address: TRIUMF, 4004 Wesbrook Mall, Vancouver, British Columbia V6T 2A3, Canada.
‡Present address: Diamond Light Source, Harwell Science and Innovation Campus, Didcot, Oxfordshire, OX11 0DE, United Kingdom.

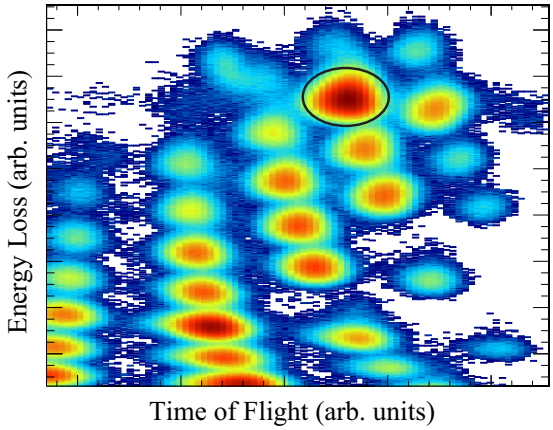

FIG. 1. Particle identification spectrum for ^{25}Si produced in the one-neutron removal from ^{26}Si on a ^{9}Be target. The energy loss was measured with the ionization chamber of the S800 focal plane and the time of flight was taken between two plastic scintillators located in the beam line and the back of the S800 focal plane. All reaction products, including ^{25}Si, are cleanly separated and identifiable. ^{25}Si is circled.

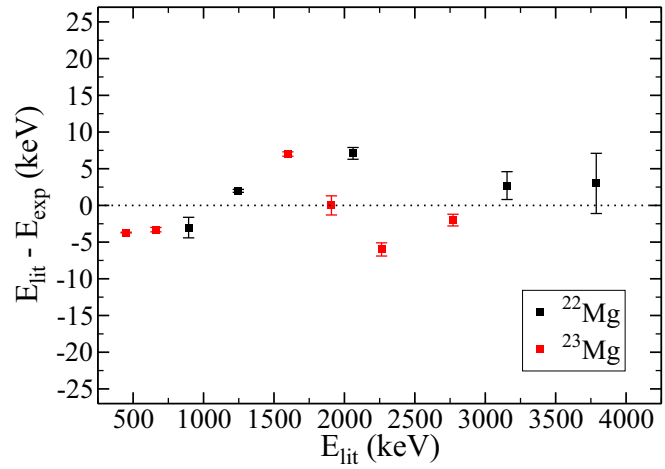

FIG. 2. Comparison of experimental (E_{exp}) and literature [23] (E_{lit}) energies for γ-ray transitions in ^{22}Mg and ^{23}Mg to determine the systematic uncertainty in Doppler-corrected energy for CAESAR. The error bars represent the uncertainty in the fit of the centroid.

was separated in flight in the A1900 fragment separator [18] using a 250 mg/cm^2 Al wedge degrader.

^{26}Si at 118 MeV/u and ^{25}Al at 111 MeV/u were then impinged on a 287(3) mg/cm^2 ^{9}Be secondary target at the reaction target position of the S800 spectrograph [19]. Event-by-event particle identification in the entrance and exit channel used timing detectors and the standard set of S800 focal-plane detectors [20] as illustrated in some detail in Fig. 1 of Ref. [21]. For the measurement presented here, the particle identification spectrum for reaction residues induced by ^{26}Si in the incoming beam is shown in Fig. 1. For this measurement, the magnetic field of the S800 was tuned to center the two-neutron knockout reaction residues from ^{25}Al and ^{26}Si projectiles, respectively. The large acceptance of the S800 spectrograph allowed detection of ^{25}Si produced from the same projectiles as well.

The secondary target was surrounded by CAESAR [22], a high-efficiency array consisting of 192 CsI(Na) scintillators, to measure deexcitation γ rays from the reaction channels of interest ^{9}Be(^{26}Si,^{25}Si)X and ^{9}Be(^{25}Al,^{25}Si)X. The high granularity of CAESAR enabled event-by-event Doppler reconstruction of the γ rays emitted in flight. GEANT4 simulations were performed to model the in-beam response of CAESAR after Doppler-shift correction, benchmarked against spectra measured with various standard calibration sources in the laboratory frame.

The systematic uncertainty for γ-ray energies in ^{25}Si measured by CAESAR in-beam was evaluated by comparing energies of known γ rays [23] to the experimental values obtained after Doppler reconstruction. High-statistics transitions with known short lifetimes from the reaction channels ^{9}Be(^{24}Mg,^{22}Mg+γ)X and ^{9}Be(^{24}Mg,^{23}Mg+γ)X were utilized. The results are shown in Fig. 2. The 4.5 keV standard deviation was adopted as the systematic uncertainty in the Doppler-corrected energy. This uncertainty was added in quadrature to the fit uncertainties.

In order to resolve the transitions to the ground state and to the known low-lying first excited state [10], high-resolution γ-ray data collected for ^{25}Si with SeGA [24], an array of high-purity 32-fold segmented germanium detectors, were utilized. For this, two existing data sets of ^{9}Be(^{26}Si,^{25}Si+γ)X were combined. These measurements were taken within the same experimental scheme described above, only that the γ-ray detection was performed with SeGA instead of CAESAR. The full technical details are given in Refs. [21] and [25]. For the new experiment presented here and the data set corresponding to Ref. [21], the ^{25}Si residues were not fully within the S800 acceptance, preventing extraction of spectroscopic factors and ℓ values from a one-nucleon knockout analysis.

In Ref. [21], a secondary beam including ^{26}Si was produced by fragmentation of a 150 MeV/u ^{36}Ar primary beam on a ^{9}Be production target at the midacceptance target position of the A1900. The secondary beam was purified using a 300 mg/cm^2 Al wedge degrader and momentum slits at the dispersive image of the A1900 and was impinged on a 188(4) mg/cm^2 ^{9}Be target at the reaction target position of the S800, which was tuned to center one-neutron knockout reaction residues from ^{28}S [21].

Similarly, in Ref. [25], a 150 MeV/u ^{36}Ar primary beam was fragmented on a ^{9}Be production target at the midacceptance position of the A1900 to produce a secondary beam including ^{26}Si. The secondary beam was impinged on a 376(4) mg/cm^2 ^{9}Be target at the reaction target position of the S800, which was tuned to center one- and two-neutron knockout residues from ^{26}Si, respectively [25,26]. For the setting that was actually optimized for ^{25}Si, the one-neutron knockout analysis of the lowest-lying states is presented in Ref. [25] and compared to USDB shell-model calculations, however, the higher-lying states important here escaped observation due to low statistics.

III. RESULTS

The Doppler-corrected γ-ray spectra of ^{25}Si produced from the CAESAR data are shown in Fig. 3 for each reaction

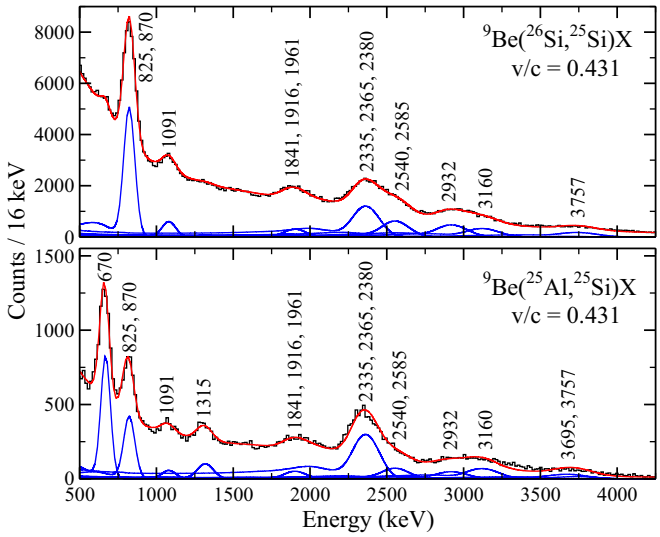

FIG. 3. Doppler-corrected γ-ray spectra from CAESAR in coincidence with ^{25}Si from the two different reactions. The spectra were fit with GEANT4 simulations of the observed peaks on top of a double exponential background. Some transition energies are taken from the high-resolution data (Fig. 6).

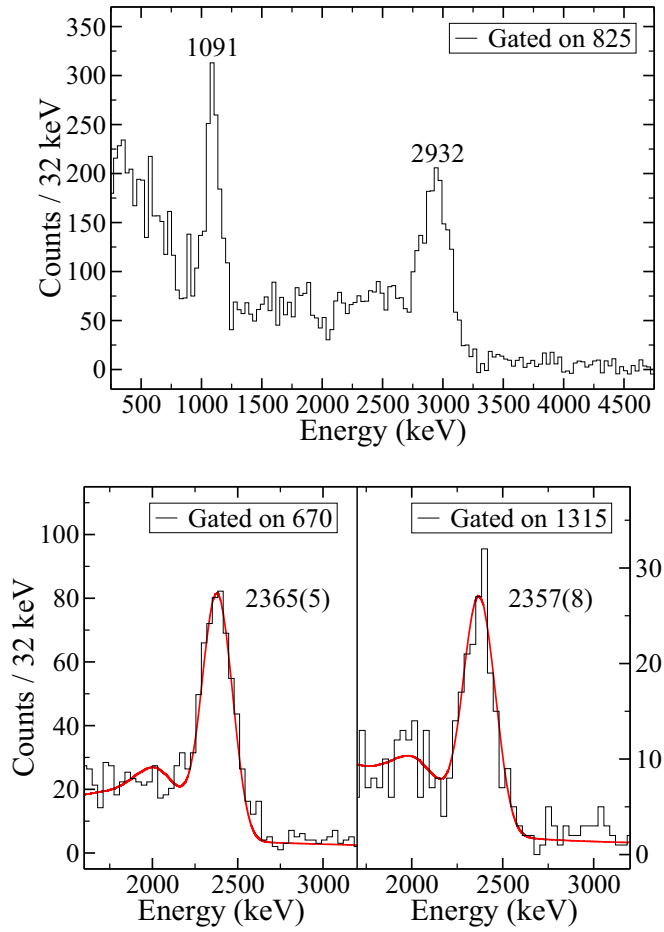

FIG. 4. Background-subtracted $\gamma\gamma$ coincidence spectra gated on the 825 keV transition from ^{9}Be(^{26}Si,^{25}Si+γ)X (top) and the 670 and 1315 keV transitions from ^{9}Be(^{25}Al,^{25}Si+γ)X (bottom) as measured with CAESAR. The solid red curves are GEANT4 simulations. The difference in energy for the peaks coincident with the 670 and 1315 keV transitions is consistent with the observation of multiple transitions in the 2365-keV region with SeGA.

channel ^{9}Be(^{26}Si,^{25}Si+γ)X and ^{9}Be(^{25}Al,^{25}Si+γ)X. The level scheme of ^{25}Si was constructed from $\gamma\gamma$ coincidences. As seen in Fig. 4, the 1091(6) and 2932(9) keV transitions are coincident with the 825(4) keV transition. The 670(5) keV transition is coincident with a peak centered at 2365 keV (5 keV fit uncertainty) while the centroid of the peak coincident with the 1315(7) keV transition is found lower in energy at 2357 keV (8 keV fit uncertainty). This is consistent with the observation of multiple transitions in the 2365-keV region in the higher-resolution SeGA data (Fig. 6) and the proposed level scheme (Fig. 7). Reverse gating within the cascade confirms the same coincidence relationships.

When summed, these coincidences suggest two potentially astrophysically relevant states near the previously reported levels at 3.7 MeV [13,14] and 3.8 MeV [10]. Supporting this is an enhancement in the detector multiplicity 1 spectrum of CAESAR as compared to the singles spectrum in this region (Fig. 5), which is for a 4π array indicative of direct transitions to either the ground state or the first excited state previously reported at 40(5) keV [10] that is expected to be isomeric from the mirror ^{25}Na, rendering it unobservable in our in-flight spectroscopy measurements.

The energies and uncertainties for the 670, 1315, and 3160 keV transitions are taken from the CAESAR data (with values for the 3160 keV transition derived from the multiplicity 1 spectrum of Fig. 5) while the energies and uncertainties for the 825, 1091, and 2932 keV transitions are from both the CAESAR and SeGA data (see Fig. 6). Energies and uncertainties for the remaining transitions were taken from the SeGA data.

The two existing high-resolution sets of ^{9}Be(^{26}Si,^{25}Si+γ)X data collected with SeGA [21,25] were analyzed to resolve the transitions to the ground state and to the low-lying first excited state in ^{25}Si. For the purpose of γ-ray spectroscopy, the two data sets were added and are shown in Fig. 6. The peaks at 825(4) and 1091(6) keV are consistent with those previously reported by Ref. [25]. The difference in energy between the 825(4) and 870(6) keV peaks gives the energy of the first excited state as 45(4) keV, which is in agreement with 40(5) keV reported in Ref. [10]. The 1091(6), 1916(7), and 1961(8) keV peaks then correspond to transitions from a level at 1961 keV to the 870 and 45 keV excited states and to the ground state. The peaks at 1841(11) and 2932(9) keV are consistent with decays from a level in the astrophysically relevant energy range at 3802(11) keV to the states at 1961 and 870 keV. This is supported by the $\gamma\gamma$ coincidence analysis using the CAESAR data described above. The statistics of the SeGA data were not sufficient for a $\gamma\gamma$ coincidence analysis. The transition at 2218(10) keV is visible in the SeGA data but not in the CAESAR data. In comparisons to shell-model calculations and experimental data on the mirror nucleus (see Fig. 7), it is likely not a transition to

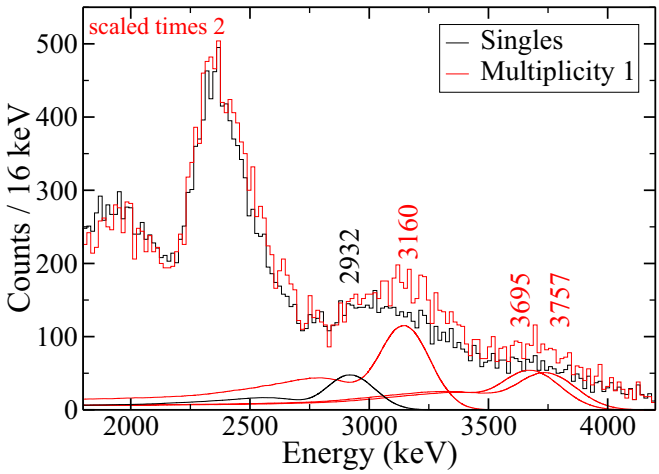

FIG. 5. Singles and multiplicity 1 spectra for γ rays measured with CAESAR from the ^{9}Be(^{25}Al,^{25}Si)X reaction and GEANT4 simulations of the labeled transitions. The 3160, 3695, and 3757 keV transitions to the ground state and low-lying first excited state (unobservable) are enhanced for multiplicity 1 as compared to the singles spectrum while the 2932 keV transition, which feeds the 870 keV state, is suppressed.

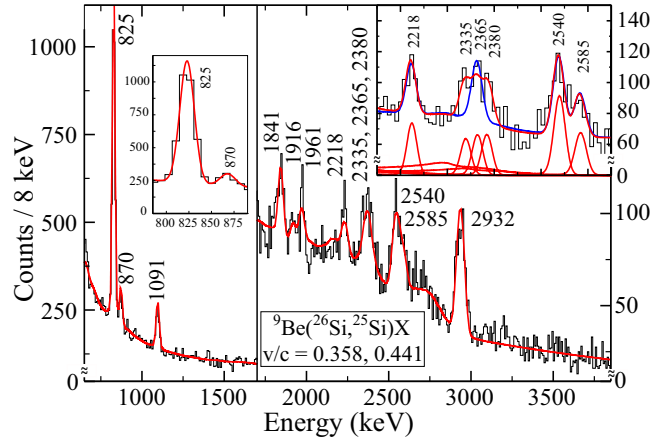

FIG. 6. Summed Doppler-corrected γ-ray spectrum of ^{25}Si measured with SeGA during the experiments described in Refs. [21] ($v/c = 0.358$) and [25] ($v/c = 0.441$). The red curve is a GEANT4 simulation of the labeled peaks on top of background. The inset expands the region around 2365 keV. The blue and red curves are simulations showing that a single peak at 2365 keV fails to describe the data.

the ground state or first excited state and originates from a higher-lying level. The 2585(12) and 2540(9) keV γ rays in the SeGA data are likely decays from a level at 2585 keV to the ground state and the level at 45 keV.

The region centered around 2365 keV cannot be described by a single peak as seen in the inset of Fig. 6. Instead, the peak structure is well described by three peaks at 2335(12), 2365(7), and 2380(12) keV. The energy difference between the 2380 and 2335 keV transitions of 45 keV suggests a level

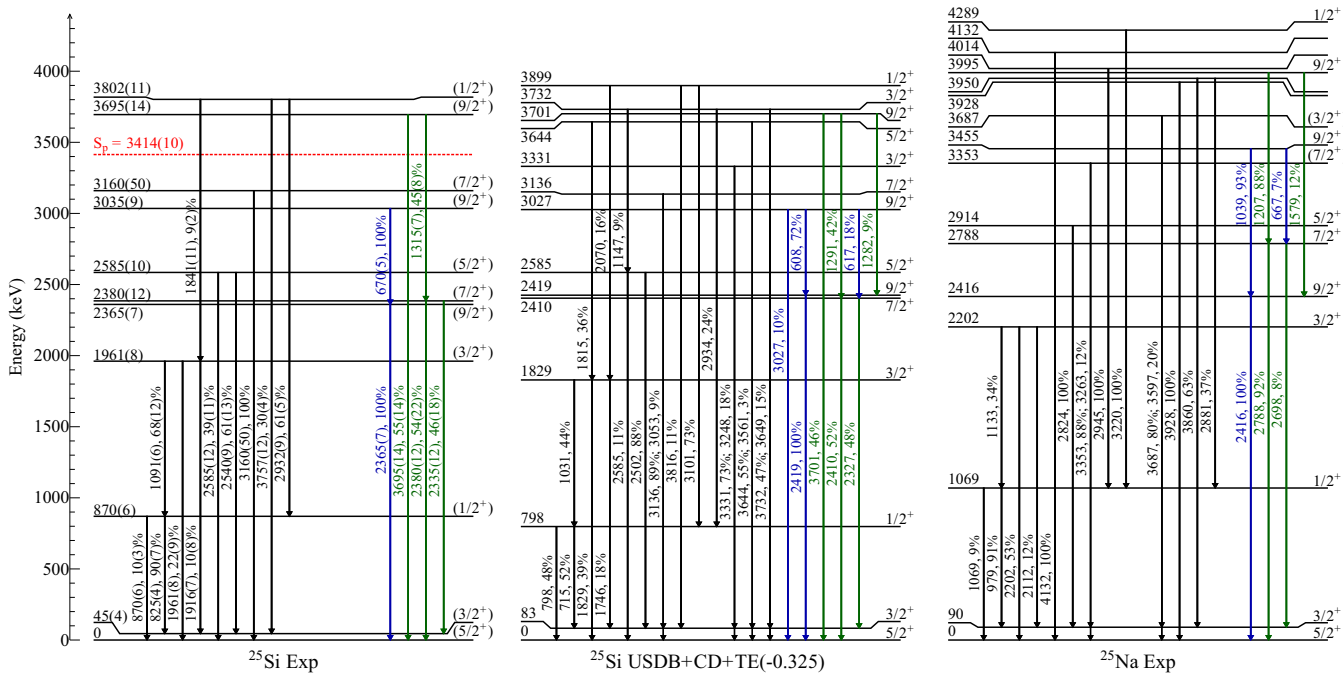

FIG. 7. Comparison of our proposed ^{25}Si energy level scheme and the γ decay branching ratios (%) to USDB+CD+TE(-0.325) shell-model calculations and the mirror nucleus ^{25}Na. Some transitions predicted by the shell-model calculations with branchings smaller than 5% are omitted. Details on the USDB+CD+TE(-0.325) interaction, which includes charge-dependent parts and a Thomas-Ehrman shift of 0.325 MeV for the proton $1s_{1/2}$ orbital, are given in Sec. IV. For ^{25}Na, branching ratios and spin-parity assignments are taken from Refs. [15] and [16] when available and otherwise taken from Ref. [23]. Transitions from the $9/2^+_2$ and $9/2^+_1$ states are indicated in blue and transitions from the $9/2^+_3$ and $7/2^+_1$ states in green to highlight the identification of the $(9/2^+)$ resonance at the center of our work.

at 2380 keV. Fitting the region from 2264–2464 keV using 8 keV per bin with a double exponential background and one peak at 2365 keV yields a reduced χ^2 of 2.1. The reduced χ^2 is lowered to 1.4 using two peaks (2345 and 2385 keV) and further lowered to 1.1 using peaks at 2335, 2365, and 2380 keV. For the fits, peak widths were held fixed and taken from GEANT4 simulations of the in-beam response of SeGA.

The γ-ray decays observed with CAESAR at 670 and 1315 keV are most similar to transitions observed in the mirror nucleus, ^{25}Na, from the $9/2^+_2$ and $9/2^+_3$ states to both the $7/2^+_1$ and $9/2^+_1$ states, as seen in Fig. 7. The spin-parities for these levels in the mirror nucleus were definitively assigned using the $d(^{24}\mathrm{Na},p)^{25}\mathrm{Na}$ reaction [16] consistent with Ref. [15]. The 670 and 1315 keV transitions were populated strongly in the $^9\mathrm{Be}(^{25}\mathrm{Al},^{25}\mathrm{Si})X$ reaction and were not observed in the SeGA experiments, in which ^{25}Si was produced from one-neutron knockout. This supports the high spin assignments suggested by the shell-model calculation and the mirror data since states in ^{25}Si with spins greater than 5/2 will not be populated directly in one-neutron knockout from ^{26}Si.

Since the 670 keV transition is coincident with a peak at 2365 keV in the CAESAR data and the γ decay of the $9/2^+_2$ level is predominately to the $9/2^+_1$ state in both the shell-model calculation and the experimental data on the mirror nucleus, the 2365 keV state observed in the SeGA data likely corresponds to the $9/2^+_1$ level (see blue transitions in Fig. 7). Similarly, the 2335 and 2380 keV transitions observed in the SeGA data are associated with the $7/2^+_1$ level, which is fed by the $9/2^+_2$ state (see green transitions in Fig. 7).

In the shell-model calculation and the mirror nucleus, the $9/2^+_2$ and $9/2^+_3$ levels have γ-decay branches to both the $9/2^+_1$ and $7/2^+_1$ states. Consequently, the 670 and 1315 keV transitions observed only in the CAESAR data could be doublets. Assuming the 670 and 1315 keV transitions observed with CAESAR are single transitions to the 2365 and 2380 keV states, respectively, places the $(9/2^+_2)$ and $(9/2^+_3)$ levels at 3035(9) and 3695(14) keV. For comparison, we can instead suppose the peaks observed with CAESAR are doublets with average energies of 670 and 1315 keV. Using the shell-model branching ratios from Fig. 7 to determine the energies of the transitions required to produce doublets with average energies of 670 and 1315 keV, the $(9/2^+_2)$ and $(9/2^+_3)$ states come out at 3038(10) and 3692(13) keV. Similarly, using the branchings from ^{25}Na gives energies of 3036(10) and 3693(13) keV. Since using the shell-model and ^{25}Na branching ratios does not significantly impact the energies compared to their uncertainties, we adopt the energies of 3035(9) and 3695(14) keV for the $(9/2^+_2)$ and $(9/2^+_3)$ levels derived from the assumption that the observed 670 and 1315 keV transitions are single transitions to the 2365 and 2380 keV states, respectively.

Branching ratios for states observed in ^{25}Si are given in Fig. 7. To calculate the branching ratios, the γ-ray singles spectra from CAESAR (Fig. 3) and SeGA (Fig. 6) were fit with GEANT4 simulations of the observed peaks on top of a double exponential background. The peak areas from these fits were corrected for the energy-dependent γ-ray detection efficiencies of CAESAR and SeGA to determine the number of γ decays. All quoted uncertainties for branching ratios include fit, statistical, and efficiency uncertainties added in quadrature.

Tentative spin-parity assignments for the observed states in ^{25}Si were made by comparison with the shell-model calculations and the mirror nucleus. The assignments are consistent with the reaction mechanisms used to populate the states aside from the weak population of the $7/2^+_1$ and $9/2^+_1$ levels observed in one-neutron knockout. These complex-structure, higher-spin levels may have been weakly populated via a two-step mechanism as discussed in Refs. [27,28].

The 3802 keV level, which is above the proton separation energy in ^{25}Si, is most similar to the $1/2^+_2$ state in the shell-model calculations and mirror nucleus. In the shell-model calculations, this state γ decays to the $1/2^+_1$, $3/2^+_1$, and $3/2^+_2$ levels with branching ratios of 73%, 11%, and 36%, while in the mirror nucleus only a decay to the $1/2^+_1$ state was observed. In this work, the 3802 keV level was found to predominantly decay to the $(1/2^+_1)$ state with a 61(5)% branching ratio and to decay to the $(3/2^+_1)$ and $(3/2^+_2)$ states with branching ratios of 30(4)% and 9(2)%.

Based on the tentative spin-parity assignments, the multiplicity 1 decays of the 3695 and 3802 keV states observed in CAESAR are to the ground and first excited states, respectively. Although the 3802 keV state is above the proton separation energy and is tentatively assigned a spin-parity of $1/2^+$, it will predominantly γ decay since it cannot proton decay in the *sd* shell to the 4^+ ground state of ^{24}Al and is energetically forbidden to proton decay to the 426 keV 1^+ state [23].

The observed γ decays to the ground state and low-lying first excited state compared to the shell-model calculation and the mirror nucleus support the ground-state spin-parity assignment of $5/2^+$ listed for ^{25}Si in Ref. [23]. In general, there is a downward shift in the energies of analog states from ^{25}Na to ^{25}Si of about 0.3 MeV, attributed in part to the Thomas-Ehrman effect since the states in ^{25}Si have some $1s_{1/2}$ overlap with low-lying states in ^{24}Al.

IV. DISCUSSION

We will discuss next the impact of the $(9/2^+)$ resonance established in this work at 3695(14) keV on the $^{24}\mathrm{Al}(p,\gamma)^{25}\mathrm{Si}$ rate. The contribution of the $(1/2^+)$ resonance at 3802(11) keV through capture on the excited 1^+ state of ^{24}Al is very small [29]. The resonant reaction rate for capture on a nucleus in an initial state i, $N_A\langle\sigma v\rangle_{\mathrm{res}\,i}$ for isolated narrow resonances is calculated as a sum over all relevant compound nucleus states f above S_p [30]:

$$N_A\langle\sigma v\rangle_{\mathrm{res}\,i} = 1.540\times10^{11}(\mu T_9)^{-3/2} \times\sum_f \omega\gamma_{if}\,\mathrm{e}^{-11.605\times E_{\mathrm{res}}/T_9}\ \mathrm{cm^3\,s^{-1}mol^{-1}}. \quad (1)$$

Here μ is the reduced mass in amu, T_9 is the temperature in GK, $E_{\mathrm{res}} = E_f - E_i$ is the resonance energy in the CoM system in MeV, and $\omega\gamma_{if}$ is the resonance strength for proton capture in MeV, given by

$$\omega\gamma_{if} = \frac{(2J_f+1)}{(2J_p+1)(2J_i+1)}\frac{\Gamma_{\mathrm{p}if}\Gamma_{\gamma f}}{\Gamma_{\mathrm{total}\,f}}. \quad (2)$$

$\Gamma_{\mathrm{total}\,f} = \Gamma_{\mathrm{p}if} + \Gamma_{\gamma f}$ is the total width of the resonance and J_i, J_p, and J_f denote total angular momenta of the target (^{24}Al),

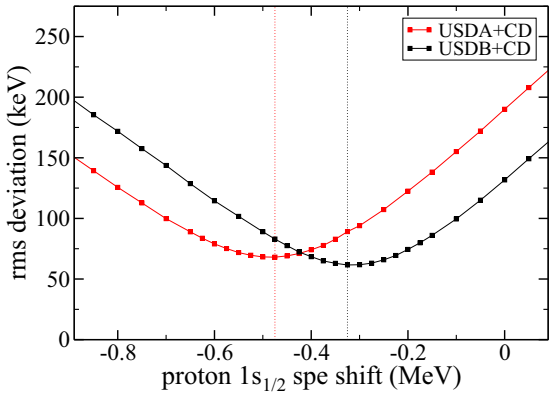

FIG. 8. Root-mean-square deviations for the experimental energies of ^{25}Si levels in Fig. 7 compared to the USDA+CD+TE and USDB+CD+TE shell-model results as functions of the proton $1s_{1/2}$ single-particle energy shift used for the TE part.

the proton projectile ($J_p = 1/2$), and states in the final nucleus (^{25}Si), respectively. The proton decay width is calculated from the proton spectroscopic factor C^2S_{if} and the single-particle proton width $\Gamma_{\mathrm{sp}if}$ as $\Gamma_{\mathrm{p}if} = C^2S_{if}\Gamma_{\mathrm{sp}if}$ where [31]

$$\Gamma_{\mathrm{sp}if} = 2\gamma^2 P(\ell, R_c), \tag{3}$$

with $\gamma^2 = \frac{\hbar^2 c^2}{2\mu R_c^2}$. A Coulomb penetration code from Barker [32] was used to calculate the barrier penetration factor $P(\ell, R_c)$. The ℓ-dependent channel radius R_c was chosen to match the widths obtained from an exact evaluation of the proton scattering cross section from a Woods-Saxon potential well. For a fixed R_c value, the simpler and computationally faster model of Eq. (3) matches the results obtained for the scattering cross sections for $Q = 0.001$–1.0 MeV to within about 10%.

We use the USDA and USDB Hamiltonians for the *sd* model space. The two Hamiltonians as well as the USD Hamiltonian discussed below are derived from singular-value-decomposition fits to energy data in the $A = 17$–40 mass region as discussed in Ref. [33]. We add to these the charge-dependent (CD) parts that were derived in Ref. [34] based on fits to isobaric mass multiplet data. We also add a Thomas-Ehrman (TE) shift for the proton $1s_{1/2}$ single-particle energy. This is to take into account the small separation energy of this orbit for proton-rich nuclei in this mass region. This shift explains the energy shifts between ^{25}Na and ^{25}Si observed in Fig. 7. As seen in Fig. 8, lowering the proton $1s_{1/2}$ single-particle energy by 0.325 MeV reduces the rms deviation between calculated and experimental level energies in ^{25}Si to 62 keV from 132 keV with no TE shift for USDB+CD. For USDA+CD, the rms deviation is 68 keV for a TE shift of 0.475 MeV compared to 190 keV for no shift. These shifts are similar to the TE shift of 0.376 MeV observed for the single-particle $1s_{1/2}$ states between ^{17}F and ^{17}O.

To explore the effect of the uncertainty in choice of TE shift on the ^{24}Al$(p,\gamma)^{25}$Si reaction rate calculation, we shift the proton $1s_{1/2}$ single-particle energy over the ranges from -0.30

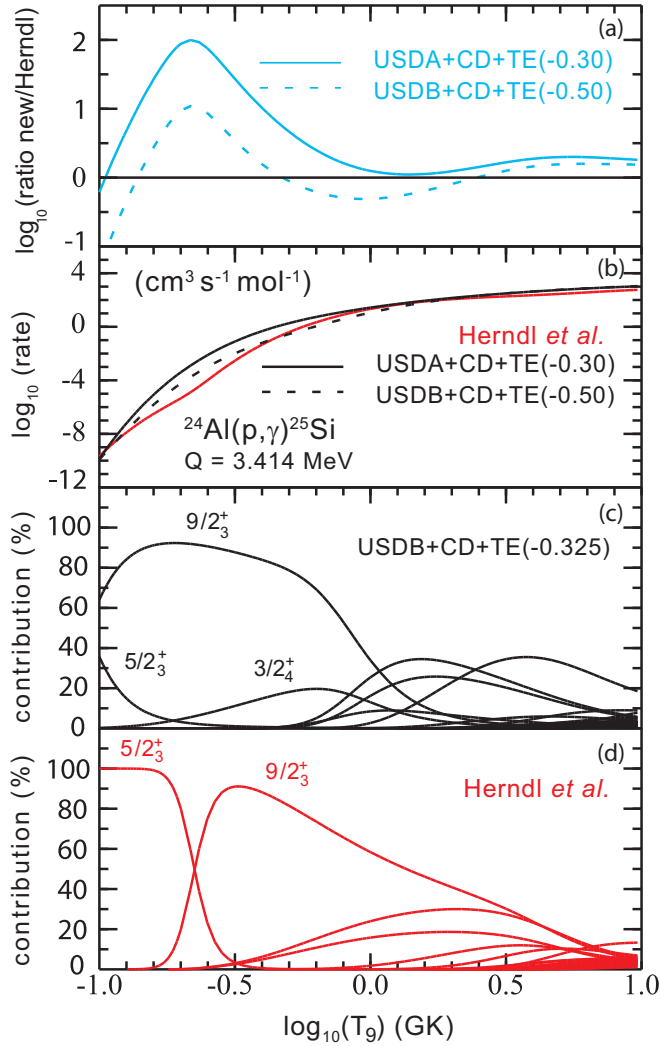

FIG. 9. (a) and (b): ^{24}Al$(p,\gamma)^{25}$Si reaction rate using the $9/2^+$ resonance from this work and the USDA/B+CD+TE interactions (black/black-dashed) compared to the results of Herndl *et al.* (red) and the resulting ratios (blue/blue-dashed). (c) and (d): individual states contributing to the rate for this work and Herndl *et al.* [3].

TABLE I. Excitation energy (E_x), spectroscopic factors for $\ell = 0$ and $\ell = 2$ (C^2S), decay widths (Γ_γ and Γ_p), and resonance strength ($\omega\gamma$) for the $9/2^+_3$ state found using different Hamiltonians.

Hamiltonian	shift MeV	E_{res}[a] keV	C^2S $\ell = 0$	C^2S $\ell = 2$	Γ_γ meV	Γ_p meV	$\omega\gamma$ meV
Herndl *et al.*	−0.11[b]	406	0.022	0.17	16	570	8.6
USDA+CD	−0.30	281	0.013	0.21	14	5.2	2.1
USDA+CD	−0.475	281	0.0055	0.20	14	9.1	4.3
USDA+CD	−0.65	281	0.0015	0.20	15	2.6	1.2
USDB+CD	−0.15	281	0.0054	0.19	15	2.3	1.1
USDB+CD	−0.325	281	0.0013	0.19	15	0.90	0.47
USDB+CD	−0.50	281	3.4×10^{-6}	0.18	15	0.50	0.27

[a]Resonance energy used to calculate the (p,γ) reaction rate.
[b]The −0.11 MeV shift in Herndl *et al.* applies to the energy of the $9/2^+_3$ state while the USDA/B shifts are for the proton $1s_{1/2}$ single-particle energy.

to −0.65 MeV and from −0.15 to −0.50 MeV for USDA and USDB, respectively. The results for these ranges together with the midpoint values are given in Table I. For USDA and USDB, the rate is obtained by fixing the energy of the $9/2^+_3$ state to its experimental energy of 3.695 MeV.

The small $C^2S(\ell = 0)$ is very sensitive to the shift as well as the Hamiltonian. $C^2S(\ell = 0)$ ranges from 0.013 for USDA with a $1s_{1/2}$ shift of −0.30 MeV down to nearly zero for USDB with a shift of −0.50 MeV. The rate for these two extremes is shown in Fig. 9 in comparison with the rate obtained by Herndl *et al.* using the USD+CD Hamiltonian plus some small energy shifts for individual states [3].

Our results differ from those of Herndl *et al.* for several reasons. We now have experimental information on the energy of levels in ^{25}Si. We find that the energy shift between ^{25}Si and ^{25}Na of the $9/2^+_3$ state is larger than the value of −0.11 MeV calculated by Herndl *et al.* (see Fig. 7). The main reason is that Herndl *et al.* only consider the small spectroscopic parentage to the ground state of ^{24}Al but the odd-odd nucleus ^{24}Al has a high level density at low excitation energy and many of the strong $1s_{1/2}$ spectroscopic factors for excited states in ^{25}Si are associated with low-lying levels of ^{24}Al.

Furthermore, the small value of $C^2S(\ell = 0)$ is sensitive to the Hamiltonian. We take into account the change of the spectroscopic factor due to the proton $1s_{1/2}$ energy shift. Herndl *et al.* just considered a shift of −0.11 MeV in the energy of the $9/2^+_3$ state and assumed the wave function (the spectroscopic factor) did not change.

The reason for the large shift for the $1s_{1/2}$ proton single-particle energy is that it lies close to zero separation energy in this mass region. Excited states in ^{25}Si are formed partly from the excitation of protons from $0d_{5/2}$ to $1s_{1/2}$. This will also be the case for excited states in ^{24}Si and ^{26}Si.

Even when $C^2S(\ell = 0) = 0$ for the $9/2^+_3$ state, our new rate is a factor of 10 larger than Herndl *et al.* calculated due to the energy shift of the $9/2^+_3$ state and the values of $C^2S(\ell = 2)$ and Γ_γ that are not sensitive to the Hamiltonian or the $1s_{1/2}$ energy shift.

V. SUMMARY

In summary, energy levels and branching ratios for the neutron-deficient nucleus ^{25}Si were determined from in-beam γ-ray spectroscopy with a high-efficiency scintillator array and a high-resolution HPGe detector array. Two states above the proton separation energy, a $(9/2^+)$ state at 3695(14) keV and a $(1/2^+)$ state at 3802(11) keV were identified. The USDA/B+CD interactions with 0.475 and 0.325 MeV Thomas-Ehrman shifts of the $1s_{1/2}$ proton orbital, respectively, were used to calculate the ^{24}Al$(p,\gamma)^{25}$Si reaction rate. At low temperature, the $(9/2^+)$ state provides the dominant contribution to the rate leading to a factor of 10–100 increase as compared to the rates reported in Ref. [3]. The sizable Thomas-Ehrman effect encountered here for ^{25}Si may apply to neighboring systems also, potentially strongly impacting more *rp*-process rates.

ACKNOWLEDGMENTS

This work was supported by the National Science Foundation (NSF) under Grants No. PHY-1102511 and No. PHY-1565546, by the DOE National Nuclear Security Administration through the Nuclear Science and Security Consortium, under Award No. DE-NA0003180, and by the Department of Energy, Office of Nuclear Physics, under Grant No. DE-FG02-08ER41556. B.A.B. acknowledges support from NSF Grant No. PHY-1404442. W.A.R. is supported by the National Research Foundation of South Africa Grant No. 105608. Figure 7 was created using the SciDraw figure preparation system [35].

[1] R. K. Wallace and S. E. Woosley, Astrophys. J. Suppl. **45**, 389 (1981).
[2] L. V. Wormer, J. Görres, C. Iliadis, M. Wiescher, and F.-K. Thielemann, Astrophys. J. **432**, 326 (1994).
[3] H. Herndl, J. Görres, M. Wiescher, B. A. Brown, and L. V. Wormer, Phys. Rev. C **52**, 1078 (1995).
[4] C. Iliadis, R. Longland, A. E. Champagne, A. Coc, and R. Fitzgerald, Nucl. Phys. A **841**, 31 (2010).
[5] W. A. Richter, B. A. Brown, A. Signoracci, and M. Wiescher, Phys. Rev. C **83**, 065803 (2011).
[6] W. A. Richter and B. A. Brown, Phys. Rev. C **85**, 045806 (2012).
[7] W. A. Richter and B. A. Brown, Phys. Rev. C **87**, 065803 (2013).
[8] J. L. Fisker, H. Schatz, and F.-K. Thielemann, Astrophys. J. Suppl. **174**, 261 (2008).
[9] M. Wang, G. Audi, A. H. Wapstra, F. G. Kondev, M. MacCormick, X. Wu, and B. Pfeiffer, Chin. Phys. C **36**, 1603 (2012).
[10] W. Benenson, J. Driesbach, I. D. Proctor, G. F. Trentelman, and B. M. Preedom, Phys. Rev. C **5**, 1426 (1972).
[11] C. Iliadis, A. E. Champagne, J. José, S. Starrfield, and P. Tupper, Astrophys. J. Suppl. Ser. **142**, 105 (2002).
[12] D. D. Clayton and L. R. Nittler, Annu. Rev. Astron. Astrophys. **42**, 39 (2004).
[13] M. Hosaka, S. Kubono, V. Guimaraes, S. C. Jeong, I. Katayama, T. Miyachi, T. Nomura, M. H. Tanaka, Y. Fuchi, H. Kawashima, S. Kato, C. C. Yun, T. Niizeki, S. Hamada, M. Hirai, K. Ito, A. Terakawa, H. Orihara, N. Ikeda, T. Kishida, Y. Pu, H. Miyatake, and T. Shimoda, in *Proceedings of the International Conference on the Exotic Nuclei and Atomic Masses*, edited by M. de Saint Simon and O. Sorlin (Editions Frontiéres, Gif-sur-Yvette Cedex, France, 1995), p. 691.
[14] S. Kubono, M. Hosaka, P. Strasser, V. Guimaraes, S. C. Jeong, I. Katayama, T. Miyachi, T. Nomura, M. H. Tanaka, Y. Fuchi, H. Kawashima, S. Kato, C. C. Yun, H. Orihara, T. Niizeki, H. Miyatake, T. Shimoda, T. Kajino, and S. Wanajo, Nucl. Phys. A **621**, 195 (1997).
[15] J. M. VonMoss, S. L. Tabor, V. Tripathi, A. Volya, B. Abromeit, P. C. Bender, D. D. Caussyn, R. Dungan, K. Kravvaris, M. P. Kuchera, R. Lubna, S. Miller, J. J. Parker IV, and P.-L. Tai, Phys. Rev. C **92**, 034301 (2015).
[16] A. Knapton, Ph.D. thesis, University of Surrey, 2017 (unpublished).

[17] A. Gade and B. M. Sherrill, Phys. Scr. **91**, 053003 (2016).
[18] D. J. Morrissey, B. M. Sherrill, M. Steiner, and I. Wiedenhoever, Nucl. Instrum. Methods Phys. Res. B **204**, 90 (2003).
[19] D. Bazin, J. A. Caggiano, B. M. Sherrill, J. Yurkon, and A. Zeller, Nucl. Instrum. Methods Phys. Res. B **204**, 629 (2003).
[20] J. Yurkon, D. Bazin, W. Benenson, D. J. Morrissey, B. M. Sherrill, D. Swan, and R. Swanson, Nucl. Instrum. Methods Phys. Res. A **422**, 291 (1999).
[21] A. Gade, P. Adrich, D. Bazin, M. D. Bowen, B. A. Brown, C. M. Campbell, J. M. Cook, T. Glasmacher, P. G. Hansen, K. Hosier, S. McDaniel, D. McGlinchery, A. Obertelli, K. Siwek, L. A. Riley, J. A. Tostevin, and D. Weisshaar, Phys. Rev. C **77**, 044306 (2008).
[22] D. Weisshaar, A. Gade, T. Glasmacher, G. F. Grinyer, D. Bazin, P. Adrich, T. Baugher, J. M. Cook, C. Aa. Diget, S. McDaniel, A. Ratkiewicz, K. P. Siwek, and K. A. Walsh, Nucl. Instrum. Methods Phys. Res. A **624**, 615 (2010).
[23] Evaluated Nuclear Structure Data File (ENSDF), http://www.nndc.bnl.gov/ensdf.
[24] W. F. Mueller, J. A. Church, T. Glasmacher, D. Gutknecht, G. Hackman, P. G. Hansen, Z. Hu, K. L. Miller, and P. Quirin, Nucl. Instrum. Methods Phys. Res. A **466**, 492 (2001).
[25] R. R. Reynolds, P. D. Cottle, A. Gade, D. Bazin, C. M. Campbell, J. M. Cook, T. Glasmacher, P. G. Hansen, T. Hoagland, K. W. Kemper, W. F. Mueller, B. T. Roeder, J. R. Terry, and J. A. Tostevin, Phys. Rev. C **81**, 067303 (2010).
[26] K. Yoneda, A. Obertelli, A. Gade, D. Bazin, B. A. Brown, C. M. Campbell, J. M. Cook, P. D. Cottle, A. D. Davies, D.-C. Dinca, T. Glasmacher, P. G. Hansen, T. Hoagland, K. W. Kemper, J.-L. Lecouey, W. F. Mueller, R. R. Reynolds, B. T. Roeder, J. R. Terry, J. A. Tostevin, and H. Zwahlen, Phys. Rev. C **74**, 021303(R) (2006).
[27] S. R. Stroberg, A. Gade, J. A. Tostevin, V. M. Bader, T. Baugher, D. Bazin, J. S. Berryman, B. A. Brown, C. M. Campbell, K. W. Kemper, C. Langer, E. Lunderberg, A. Lemasson, S. Noji, F. Recchia, C. Walz, D. Weisshaar, and S. J. Williams, Phys. Rev. C **90**, 034301 (2014).
[28] A. Mutschler, O. Sorlin, A. Lemasson, D. Bazin, C. Borcea, R. Borcea, A. Gade, H. Iwasaki, E. Khan, A. Lepailleur, F. Recchia, T. Roger, F. Rotaru, M. Stanoiu, S. R. Stroberg, J. A. Tostevin, M. Vandebrouck, D. Weisshaar, and K. Wimmer, Phys. Rev. C **93**, 034333 (2016).
[29] J. Grineviciute, B. A. Brown, and H. Schatz, arXiv:1404.7268.
[30] W. A. Fowler and F. Hoyle, Astrophys. J. Suppl. **9**, 201 (1964).
[31] A. M. Lane and R. G. Thomas, Rev. Mod. Phys. **30**, 257 (1958).
[32] F. C. Barker, Phys. Rev. C **63**, 047303 (2001); (private communication).
[33] B. A. Brown and W. A. Richter, Phys. Rev. C **74**, 034315 (2006).
[34] W. E. Ormand and B. A. Brown, Nucl. Phys. A **491**, 1 (1989).
[35] M. A. Caprio, Comput. Phys. Commun. **171**, 107 (2005).